Sensors and Actuators B 213 (2015) 322–328

Contents lists available at ScienceDirect

Sensors and Actuators B: Chemical

journal homepage: www.elsevier.com/locate/snb

Self-adhesive graphene oxide-wrapped TiO_2 nanoparticles for UV-activated colorimetric oxygen detection

Eun Jin Son[a], Joon Seok Lee[a], Minah Lee[a], Chau Hai Thai Vu[b], Hana Lee[b], Keehoon Won[b,*], Chan Beum Park[a,**]

[a] Department of Materials Science and Engineering, Korea Advanced Institute of Science and Technology (KAIST), 335 Science Road, Daejeon 305-701, Republic of Korea
[b] Department of Chemical and Biochemical Engineering, Dongguk University-Seoul, 30 Pildong-ro 1-gil, Jung-gu, Seoul 100-715, Republic of Korea

ARTICLE INFO

Article history:
Received 27 September 2014
Received in revised form 15 February 2015
Accepted 16 February 2015
Available online 25 February 2015

Keywords:
Colorimetric oxygen sensing
Graphene oxide
TiO_2 nanoparticles
Methylene blue
UV activation

ABSTRACT

We first report on the synthesis of graphene oxide-wrapped TiO_2 nanoparticles (GO-TiO_2 NPs) as a self-adhesive photocatalyst for UV-activated colorimetric oxygen detection. Methylene blue (MB), a redox dye for colorimetric oxygen indication, strongly adsorbed onto GO-TiO_2 NPs by both electrostatic and π–π stacking interactions. The chemical attraction between GO and MB significantly decreased dye leakage, which is a serious problem of colorimetric oxygen indicators; MB leaching from GO-TiO_2-based film was fivefold lower than that from conventional TiO_2-based film. This novel MB/GO-TiO_2/glycerol/hydroxyethyl cellulose film was successfully bleached by UV irradiation, and it regained its blue color rapidly in the presence of oxygen, demonstrating its useful functionality as a UV-activated colorimetric oxygen indicator.

1. Introduction

Oxygen detection is essential in medical, environmental, and food application fields because oxygen is a vital element for life, involved in a wide range of chemical/biochemical reactions [1–3]. While traditional oxygen sensing methods (e.g., electrochemical sensing, chromatographic analysis) require expensive instruments and/or trained operators, colorimetric oxygen sensors are inexpensive and simple. They allow oxygen to be detected even with the naked eye. Such oxygen indicators have received great attention especially in food packaging because oxygen is closely related to the management of food quality and safety [3]. In particular, UV-activated colorimetric oxygen indicators have the significant advantages of in-pack activation and irreversibility [4,5]. In addition, they proved to be stable for over 1 year in the dark under otherwise ambient conditions and thus have a long shelf-life under ambient conditions in marked contrast to other conventional oxygen indicators (e.g., Ageless Eye®) to require storage under anaerobic conditions [6]. Typically, they are composed of a redox dye {e.g., methylene blue (MB)}, a sacrificial electron donor (e.g., glycerol), and a UV-absorbing photocatalyst (e.g., TiO_2 nanoparticles), which are encapsulated in a polymer film {e.g., hydroxyethyl cellulose (HEC)} [3,6]. The indicator film loses its color rapidly upon exposure to UV light, remains colorless in the absence of oxygen, and regains its original color with oxygen. When in contact with water contained in food, however, the oxygen indicator film suffers from the migration of redox dyes into food, which is prohibited under the regulation; it can lead to health problems [7,8]. Many attempts have been made to address such problems [9–13]; for example, the use of hydrophobic sulfonated polystyrene (SPS) as the encapsulating polymer made the film highly resistant to dye leaching, but the MB/TiO_2/glycerol/SPS film showed very slow recovery of the color (5 days in ambient air) because of its hydrophobic property [9].

Two-dimensional carbon-based nanomaterials such as graphene (GR) and graphene oxide (GO) have drawn a great deal of attention because of their unique electrical, optical, and chemical properties [14,15]. They can also serve as a scaffold for the synthesis of functional hybrid materials through interactions with organic and inorganic chemicals [16,17]. For instance, redox dyes such as MB can be easily adsorbed onto GO sheets through π–π stacking interaction between aromatic rings of MB and sp^2-hybridized carbons of GO, as well as through ionic interaction between cationic MB and oxygen-containing functional groups

* Corresponding author. Tel.: +82 2 2260 8922.
** Corresponding author. Tel.: +82 42 350 3340.
E-mail addresses: keehoon@dongguk.edu (K. Won), parkcb@kaist.ac.kr (C.B. Park).

http://dx.doi.org/10.1016/j.snb.2015.02.084
0925-4005/

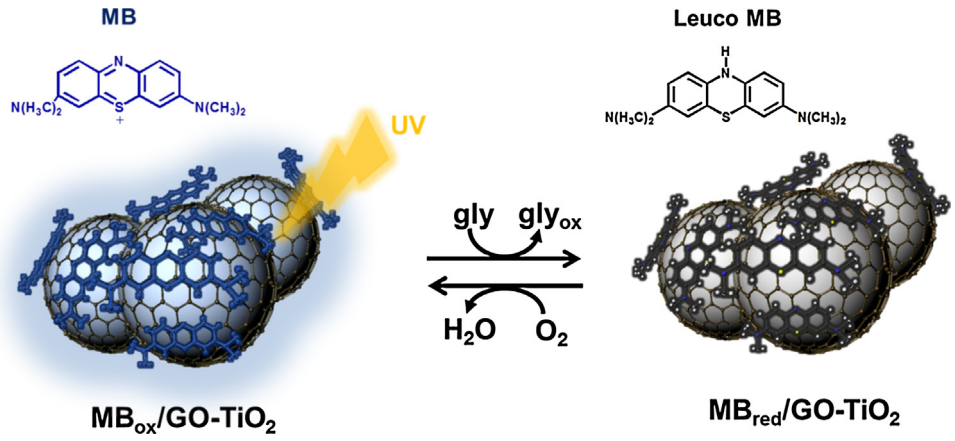

Fig. 1. Schematic illustration of photobleaching and recovery steps of MB/GO-TiO_2/glycerol/HEC oxygen indicator films.

of GO [18–21]. In this study, in order to tackle the dye leakage problem of UV-activated oxygen sensors, we have employed GO-wrapped TiO_2 nanoparticles (GO-TiO_2 NPs) as the photocatalyst for the first time, as illustrated in Fig. 1.

2. Materials and methods

2.1. Materials

Hexadecylamine (HDA, 90%), potassium chloride (KCl), titanium (IV) isopropoxide, N′-(3-trimethoxysilylpropyl) diethylenetriamine, acetic acid, HEC, glycerol, and MB were purchased from Sigma–Aldrich (St. Louis, MO, USA). GO was synthesized from graphite powder (Kropfmühl AG, Germany) according to the modified Hummers method [22].

2.2. Synthesis of GO-TiO_2 NPs

GO-wrapped TiO_2 nanoparticles were synthesized using a method modified from one described in our previous work [23]. Amorphous TiO_2 NPs were synthesized by a sol–gel method using titanium (IV) isopropoxide as a precursor; HDA (5.27 g) was dispersed in ethanol (800 ml) to which 0.1 M KCl (3.2 ml) and titanium (IV) isopropoxide (17.6 ml) were added. After incubating the mixture at room temperature for 18 h, the synthesized amorphous TiO_2 NPs were washed with ethanol several times sufficiently. In order to crystallize them to anatase TiO_2 NPs, amorphous TiO_2 NPs (0.4 g) were suspended in a mixture of ethanol (20 ml) and deionized water (10 ml). After a hydrothermal process at 160 °C for 16 h in a Teflon-lined autoclave, a calcination process was carried out in the air at 500 °C for 2 h. For wrapping of TiO_2 NPs in GO, the anatase TiO_2 surface was first modified with amine-functional groups to obtain a positive surface charge; anatase TiO_2 NPs (200 mg) were added to a mixed solution of N′-(3-trimethoxysilylpropyl) diethylenetriamine (0.8 ml), acetic acid (0.8 ml), and deionized water (40 ml). After being stirred for 4 h, the positively charged anatase TiO_2 NPs were washed by ethanol three times, then mixed with a negatively charged GO suspension (0.2 mg/ml) with the weight ratio of GO to TiO_2 NPs (0.01) under vigorous stirring. After 1 h, the resultant GO-TiO_2 NPs were separated by centrifugation and washed thoroughly with deionized water.

2.3. MB adsorption onto GO-TiO_2 NPs

For the comparison of MB adsorption onto GO-TiO_2 and anatase TiO_2 NPs, 25 mg of each NP was placed in 60 μM MB solution (4 ml). After 24 h incubation – it was reported to take about 6 h for MB to adsorb onto GO following a pseudo-second-order kinetic model [21] – the NPs were separated by centrifugation at 6000 rpm and washed with deionized water several times. The supernatant of each washed solution was monitored using a UV–Vis spectrophotometer, and the amount of MB adsorbed onto GO-TiO_2 or anatase TiO_2 NPs was calculated using the mass balance of MB.

2.4. Preparation of MB/GO-TiO_2/glycerol/HEC film

GO-TiO_2 NPs (25 mg) were dispersed in 60 μM MB solution (4 ml) and incubated with continuous stirring for 24 h. Afterwards the NPs were centrifuged at 6000 rpm and washed to remove unadsorbed MB and rinsed with deionized water. The washing process was repeated several times until no MB was observed in the supernatant of the mixture using a UV–Vis spectrophotometer. The 25 mg of MB-adsorbed GO-TiO_2 NPs (MB/GO-TiO_2 NPs) dispersed in deionized water (1.2 ml) was mixed with glycerol (20 μl) and 5 wt% HEC solution (0.5 ml). This resultant ink mixture (0.1 ml) was cast on an 18 mm diameter glass cover slip with a drop casting method, then subjected to drying at 40 °C for 30 min to be MB/GO-TiO_2/glycerol/HEC film. The formulation of the ink mixture was derived from the literature [24] and further optimized to have the best viscosity for drop casting. The final oxygen indicator film on the glass was flexible and soft, and not susceptible to cracking.

2.5. Dye leakage test of MB/GO-TiO_2/glycerol/HEC film

Twenty-five milligrams of anatase TiO_2 NPs were dispersed in 1.2 ml of MB solution, and then the dispersion was mixed with glycerol (20 μl) and 5 wt% HEC solution (0.5 ml). The MB/TiO_2/glycerol/HEC film was prepared so that it could have the same amount of MB as the pre-synthesized MB/GO-TiO_2/glycerol/HEC film. The MB/GO-TiO_2/glycerol/HEC film or MB/TiO_2/glycerol/HEC film was immersed in 5 ml of deionized water, and at 10 min intervals, MB leaching was quantified by measuring the absorbance of the supernatant at 665 nm after centrifugation.

2.6. Photobleaching and recovery behaviors of MB/GO-TiO_2/glycerol/HEC oxygen indicator film

The photobleaching reaction of the MB/GO-TiO_2/glycerol/HEC film was carried out under UV irradiation using a CL-1000 UV cross-linker (UVP, Upland, CA, USA) equipped with five tubes of UVA lamps (wavelength: 365 nm) for 1.2 min, and then the irradiation intensity measured using a digital UVX radiometer (UVP, Upland, CA, USA) was 0.4 mW/cm^2. For the recovery test, the film

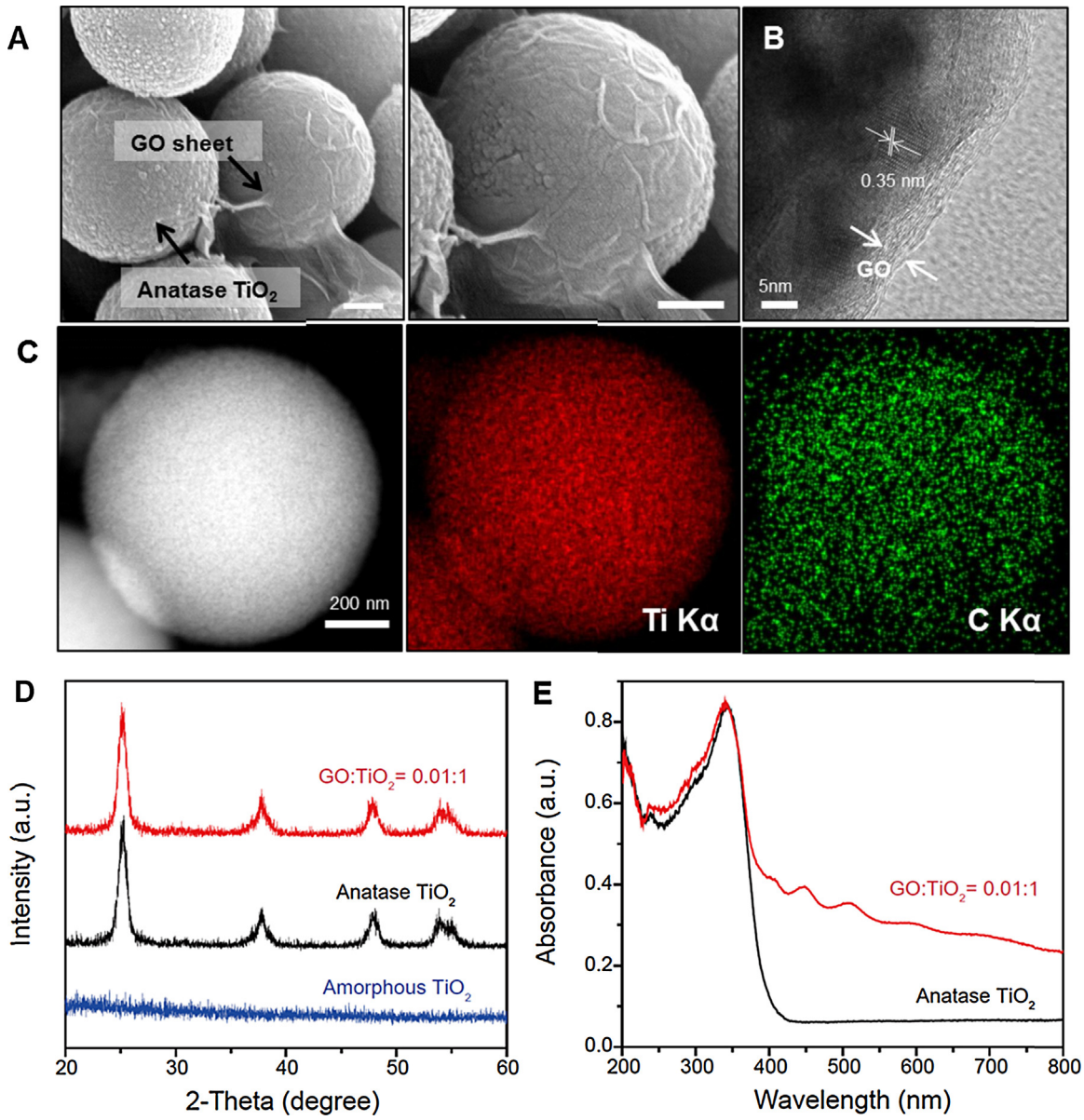

Fig. 2. (A) SEM images of GO-TiO_2 NPs with different magnification. The weight ratio of GO in GO-TiO_2 NPs was 0.01:1. Scale bar: 200 nm. (B) STEM images of GO-TiO_2 NPs. (C) Energy dispersive X-ray spectroscopy images of GO-TiO_2 NPs. Elemental mapping of Ti and C is shown in red and green respectively. (D) X-ray diffraction patterns of amorphous TiO_2 NPs, anatase TiO_2 NPs, and GO-TiO_2 NPs. (E) UV–Vis spectra of anatase TiO_2 NPs and GO-TiO_2 NPs. (For interpretation of the references to color in this figure legend, the reader is referred to the web version of this article.)

was placed in a cell where the oxygen concentration was kept around 2 or 10% using an automatic gas mixing system (Sehwa Hightech Co., Bucheon, Korea). For 21% oxygen, ambient air was used. The oxygen concentration in the gas cell was checked using an oxygen sensor (CheckPoint II, PBI-Dansensor, Denmark). The relative humidity (RH) in the cell was controlled about 11, 30, or 52% with saturated salt solutions [25], and the temperature was kept at 10, 20, or 30 °C in a temperature-controlled chamber (TH-ME-025, Jeiotech, Daejeon, Korea). The relative humidity and temperature were checked using a 4185 Traceable® Memory Hygrometer/Thermometer (Control Company, Friendswood, TX, USA).

For color change measurement, the diffuse reflectance of the MB/GO-TiO_2/glycerol/HEC film was measured using a CM-2600d portable spectrophotometer (Konica Minolta, Tokyo, Japan) and expressed in the Kubelka–Munk function [11,26]:

$$\theta = f(R'_\infty) = \frac{(1 - R'_\infty)^2}{2R'_\infty} = \alpha bC$$

where R'_∞ is the percentage reflectance relative to a white standard reflectance plate; α is the molar absorption coefficient of the dye; C is its concentration; b is a constant. When plotted against wavelength, this function generates a spectrum similar to the absorbance spectrum [27].

2.7. Characterization

The morphology and size of NPs were observed using the S-4800 field emission scanning electron microscope (SEM, Hitachi Co., Japan) and the JEM-ARM200F Cs-corrected scanning transmission electron microscope (STEM, JEOL Ltd., Japan), which were operated at 200 kV. Energy dispersive X-ray spectroscopy analysis was performed using the same Cs-corrected STEM. The crystal structure of TiO_2 NPs was determined using a D/Max-RB 12 kW X-ray diffractometer (XRD, Rigaku Co., Japan) at a scan speed of 6°/min, Cu Kα radiation wavelength of 1.5418 Å. Zeta potentials of NPs were investigated with Zetasizer Nano ZS (Malvern Ltd.,

England), and all NPs and GO samples were prepared in a concentration of 0.025 mg/ml. The UV–Vis absorption spectra of TiO_2 NPs were observed using a V/650 spectrophotometer (JASCO Inc., Japan). For cyclic voltammetry (CV), glassy carbon (GC) electrode as working electrodes was coated with 40 μl of the NP solution (1 mg/ml in ethanol) and connected to a WMPG1000 potentiostat–galvanostat (WonATech, Seoul, Korea) with Ag/AgCl reference electrode and platinum wire counter electrode. Cyclic voltammograms were obtained in 0.1 M phosphate buffer (pH 7) at room temperature at a scan rate of 100 mV/s. For the estimation of binding affinity of MB for GO, the CV measurement was repeated 100 times without interruption in 0.1 M phosphate buffer (pH 7) containing 0.5 M NaCl at a scan rate of 100 mV/s. Note that 0.5 M NaCl, which is similar to an average salinity of seawater, was chosen to represent the ionic strength of food products that possess significant salt and dissolved mineral contents.

3. Results and discussion

3.1. Synthesis of GO-TiO_2 NPs

We synthesized amorphous TiO_2 NPs through a sol–gel process. The amorphous TiO_2 was crystallized to anatase TiO_2 via hydrothermal procedure and then modified with N′-(3-trimethoxysilylpropyl) diethylenetriamine to have amine-functional groups on the surface (see Fig. S1A & B for SEM images of TiO_2 NPs). We observed a significant change in the zeta potential of the amine-treated anatase TiO_2 from −10.2 to 30.8 mV (Fig. S1C), which indicates that the anatase TiO_2 was successfully functionalized with positively charged amine groups. GO-wrapped TiO_2 was obtained through electrostatic interaction between the positively charged anatase TiO_2 and the negatively charged GO, which had a surface charge of −50.6 mV (Figs. 2A & S1C). The zeta potential shift of amine-treated anatase TiO_2 after mixing with GO (from 30.8 mV in Fig. S1C to −24.1 mV in Fig. 3A) implies that most of positively charged TiO_2 NPs were covered with GO. We further confirmed the GO-wrapped TiO_2 NPs with a lattice spacing of 0.35 nm, which was assigned to (101) plane of anatase TiO_2, through the STEM image (Fig. 2B) and the elemental mapping analysis by energy dispersive X-ray spectroscopy (Fig. 2C). The XRD patterns of amorphous TiO_2, anatase TiO_2, and GO-TiO_2 NPs are shown in Fig. 2D; no peak was observed with amorphous TiO_2 NPs while all the peaks of the hydrothermally processed TiO_2 NPs were assigned to anatase TiO_2 (JCPDS, no. 21-1272). The GO-TiO_2 NPs exhibited similar XRD pattern as the anatase TiO_2 NPs, indicating that GO-wrapping did not affect the crystallinity of the pre-synthesized anatase TiO_2 NPs. According to the UV–Vis spectra of anatase TiO_2 NPs and GO-wrapped anatase TiO_2 NPs (Fig. 2E), the absorption edge of GO-TiO_2 NPs did not shift from that of anatase TiO_2 NPs, which indicates the absorbance range of anatase TiO_2 NPs was not influenced by GO wrapping.

3.2. MB binding to GO-TiO_2 NPs

We examined the binding of MB to GO-wrapped TiO_2 NPs using zeta potential measurement and electrochemical analysis. For the test, the same amounts of GO-TiO_2 NPs and anatase TiO_2 NPs were immersed in a MB solution under continuous stirring for 24 h, and the amounts of MB adsorbed onto GO-TiO_2 NPs and anatase TiO_2 NPs were calculated using mass balance of MB. After washing, we found the loading amount of MB was 2.34 mg/g for GO-TiO_2 NPs, whereas no MB was adsorbed onto anatase TiO_2 NPs (Fig. S2), which indicates that GO ad-layer had a critical effect on MB adsorption. Fig. 3A shows that the initial zeta potential of GO-TiO_2 NPs was shifted from −24.1 to −6.48 mV after their immersion in MB

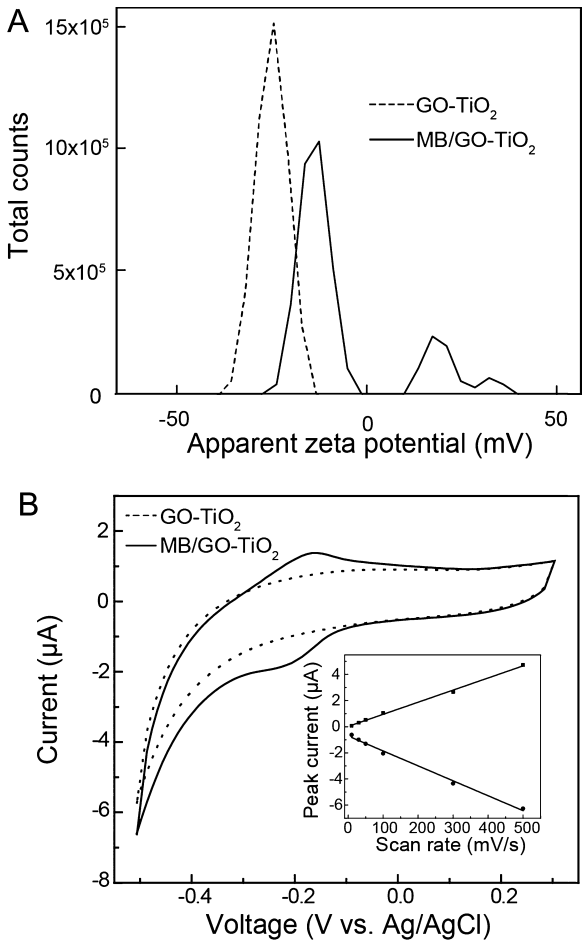

Fig. 3. (A) Surface zeta potentials of GO-TiO_2 NPs and MB/GO-TiO_2 NPs. (B) Cyclic voltammograms of GO-TiO_2 NPs (dashed line) and MB/GO-TiO_2 NPs (solid line) in 0.1 M phosphate buffer (pH 7) at a scan rate of 100 mV/s. Inset shows the plot of the redox peak currents vs. scan rates of 10, 30, 50, 100, 300, and 500 mV/s.

solution, indicating that MB, a well-known cationic dye molecule, was adsorbed onto the negatively charged GO-TiO_2 NP surface. To obtain another evidence for MB adsorption onto GO-TiO_2 NPs, we performed cyclic voltammetric analysis of the GC electrode modified with GO-TiO_2 or MB/GO-TiO_2 NPs in a phosphate buffer (0.1 M, pH 7.0). As shown in Fig. 3B, no redox peak appeared for GO-TiO_2 NPs, whereas MB/GO-TiO_2 NPs exhibited apparent anodic peak at −0.16 V (vs. Ag/AgCl) and cathodic peak at −0.22 V (vs. Ag/AgCl) attributed to two-electron and one-proton redox behavior of MB [28,29]. In addition, Fig. 3B (inset) reveals that the peak currents of the GC electrode covered with MB/GO-TiO_2 were linearly proportional to the scan rate, which is a typical characteristics of surface-confined electrochemical behavior [30,31]; the redox peaks result from MB on the electrode surface.

In order to estimate the binding affinity of MB for GO-TiO_2, we monitored the peak currents of the MB/GO-TiO_2 electrode with repeating the potential cycle 100 times without interruption. This CV experiment was carried out in 0.1 M phosphate buffer (pH 7) containing 0.5 M NaCl – salts may disturb the ionic interaction between the dye and the graphene oxide layer. During the 100 cycles, the cathodic peak currents were kept above 97% of that measured at the first cycle (Fig. 4A). After the 100 repeated cycles, the redox peak currents of the MB/GO-TiO_2 electrode were measured at different scan rates from 10 to 500 mV/s. The linear relation of the peak currents to scan rates shown in Fig. 4B indicates that the electrochemical reactions originated from MB on the electrode, not MB in the solution, revealing that MB did not leach out during the

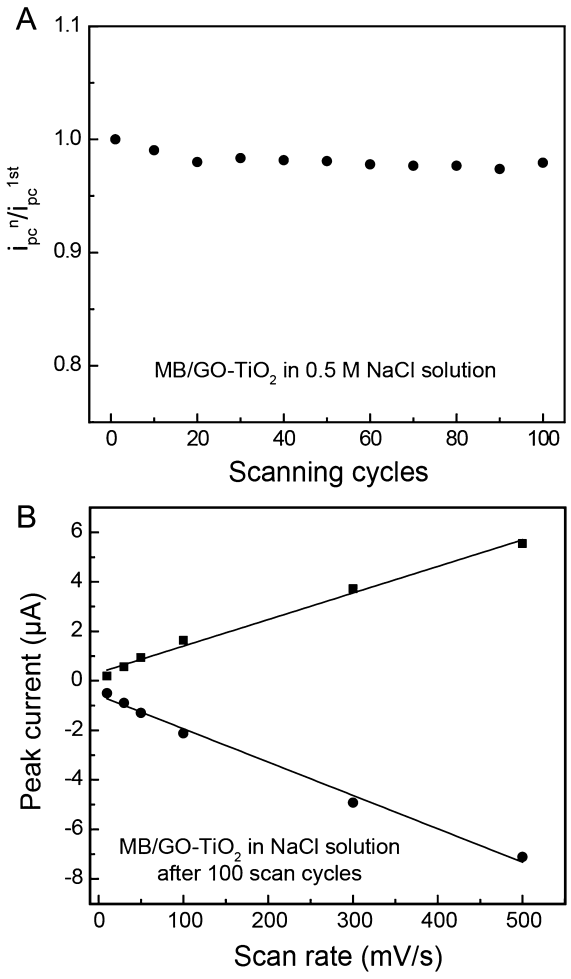

Fig. 4. (A) Cathodic current peak ratio of MB/GO-TiO_2 NPs in 0.1 M phosphate buffer (pH 7) containing 0.5 M NaCl during the 100 cycles. (B) Redox peak currents at different scan rates (10, 30, 50, 100, 300, and 500 mV/s) after the 100 scan cycles of MB/GO-TiO_2 in 0.1 M phosphate buffer (pH 7) containing 0.5 M NaCl.

100 cycles. Moreover, cyclic voltammograms of bare GC electrode in the fresh solution (Fig. S3A) and in the buffer solution after the 100 cycles (Fig. S3B) were similar. This result shows that little or no MB was present in the solution after the 100 cycles, confirming that MB did not desorb from GO-TiO_2 particles. In the same manner, the GC electrode modified with MB/GO-TiO_2 NPs was also tested in 0.1 M phosphate buffer (pH 7) devoid of NaCl; the same results were obtained (data not shown), demonstrating that 0.5 M NaCl has little or no effect on the binding between MB and GO-TiO_2 particles.

Fig. 4 suggests stable binding between MB and GO-TiO_2 nanostructure, implying that GO wrapping around TiO_2 NPs may solve the aforementioned dye leakage problem of oxygen indicator films. To test this possibility, we prepared a MB/GO-TiO_2-based film and analyzed MB leakage from the film in comparison with MB-mixed TiO_2 (MB/TiO_2)-based film without a GO layer (Fig. 5). Note that the MB/TiO_2-based film was prepared so that it could have the same amount of MB as the MB/GO-TiO_2-based film. When the MB/TiO_2-based film was immersed in water for 70 min, about 45% of MB leached into water, while only 9% of MB leaked out from the MB/GO-TiO_2-based film. This result shows that the GO wrapping around TiO_2 NPs significantly diminished the MB leakage and thus made the film resistant to dye leakage in aqueous media. For reference, this upward trend in the dye leakage continued beyond the 70 min around which we observed the hydrophilic polymer (HEC) starting to dissolve with the naked eye. It should be possible to suppress

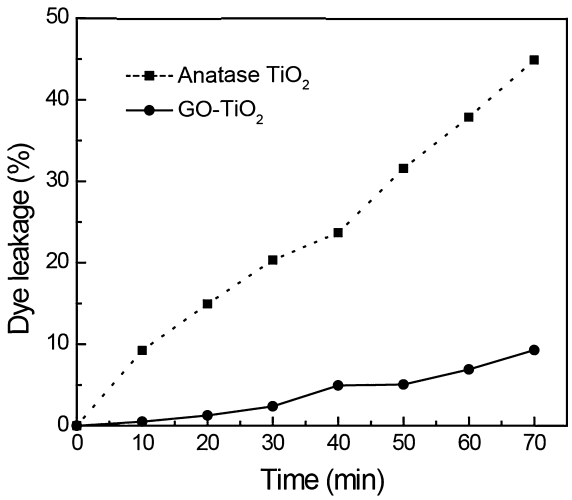

Fig. 5. Time–course profiles of the percentage of MB leaching from the MB/TiO_2- and MB/GO-TiO_2-based films.

the dye leakage of the MB/GO-TiO_2-based film in water to a greater degree by employing anionic polymers to interact with cationic MB as the encapsulating polymer [12,13].

3.3. Colorimetric oxygen detection with MB/GO-TiO_2-based film

Finally, we examined whether our new MB/GO-TiO_2-based film could act as a UV-activated oxygen indicator. Fig. 1 illustrates key steps of the MB/GO-TiO_2/glycerol/HEC oxygen indicator film. Once GO-TiO_2 NP is excited by UV light irradiation, electron-hole pairs are created, and glycerol simultaneously donates electrons to TiO_2 NPs, leaving the excited electrons in the conduction band of TiO_2. The generated electrons are immediately used to reduce MB to colorless leuco MB (LMB), bleaching its initial blue color (photobleaching step). When the film is exposed to oxygen, the color of the film returns to blue as LMB is oxidized back to its original form (recovery step). Exposure to the UVA radiation bleached the as-synthesized MB/GO-TiO_2/glycerol/HEC film successfully (data not shown). Right after the photobleaching reaction, the recovery process under aerobic conditions (21% oxygen, ~52% RH, and 30 °C) was monitored over time. In Fig. 6A, the Kubelka–Munk function at the wavelength of maximum absorption (θ_{max}), which is related to the concentration of the oxidized dye (MB), is plotted as a function of recovery time. The recovery reaction was completed within 20 min, and the photobleached MB/GO-TiO_2/glycerol/HEC film successfully regained its blue color as LMB was reoxidized to blue MB. This color recovery is significantly rapid, considering the other leaching-resistant indicator films based on hydrophobic polymers showed the recovery times of 5 days with SPS [9] and 2.5 days with low-density polyethylene [27].

Effects of oxygen concentration, temperature, and relative humidity on the recovery process were also investigated. Fig. 6B shows the initial recovery rate of the MB/GO-TiO_2/glycerol/HEC film as a function of oxygen concentration. The recovery rate was proportional to the oxygen level in the gas phase as reported in the literature [6,9,26,27,32]. The direct relationship between the rate and oxygen concentration is not unexpected recalling the dark color recovery is a reaction of LMB with oxygen ($2LMB + O_2 \rightarrow 2MB^+ + 2OH^-$). As can be seen in Fig. 6C, the initial rate of the color recovery was also dependent on temperature; the more rapidly the film responded to oxygen, the higher the temperature was as expected [10,27]. An activation energy calculated using the Arrhenius equation was 40 kJ/mol, which was not quite different from the value of 54 ± 4 kJ/mol reported in the literature

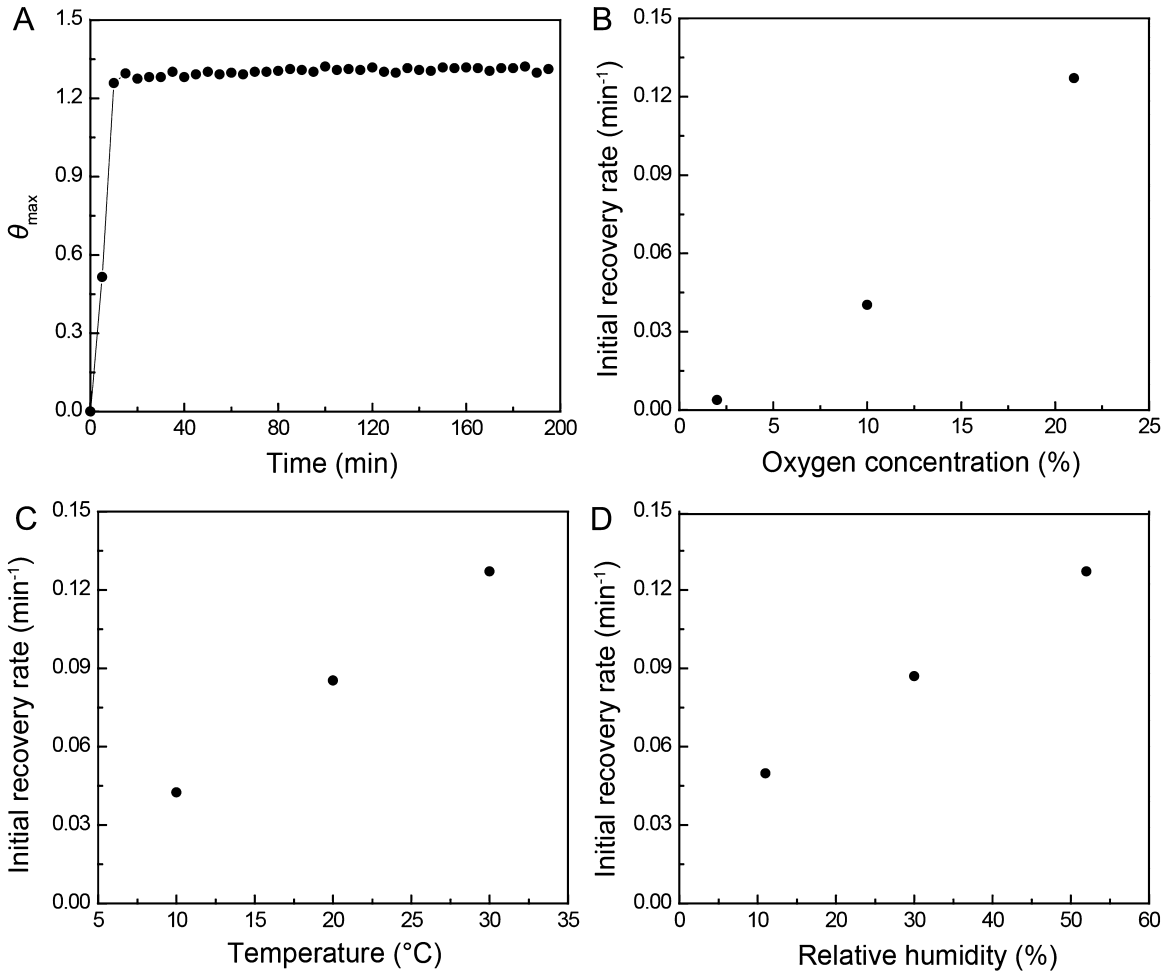

Fig. 6. (A) Recovery behavior of the MB/GO-TiO_2/glycerol/HEC oxygen indicator film in the air (~52% RH and 30 °C): the plot of the Kubelka–Munk function at the wavelength of maximum absorption (θ_{max}) vs. time. (B) Effect of oxygen concentration on the initial recovery rate (~52% RH and 30 °C). (C) Effect of temperature on the initial recovery rate (~52% RH in the air). (D) Effect of relative humidity on the initial recovery rate (30 °C in the air).

[32]. Effect of relative humidity on the initial recovery rate is depicted in Fig. 6D. The rate increased with raising RH, indicating water plays important roles in the recovery process. Water may stabilize the ionic products of the recovery reaction (i.e., MB^+ and OH^-) and increase the rate of oxygen diffusion within the film [6,9,10,32].

4. Conclusions

We have synthesized GO-TiO_2 NPs as a self-adhesive photocatalyst for UV-activated colorimetric oxygen indicator film for the first time. MB was effectively adsorbed onto GO-TiO_2 surface through chemical interactions such as electrostatic interaction and π–π electron coupling. Our analyses revealed that the chemical conjugation between GO and MB significantly diminished MB leakage, which is regarded as a serious problem of colorimetric oxygen indicators; the MB leaching from the MB/GO-TiO_2-based film was fivefold lower than that from the MB/TiO_2-based film. This novel film was successfully photobleached by UV irradiation and regained its blue color rapidly in the presence of oxygen, demonstrating that the MB/GO-TiO_2/glycerol/HEC film successfully functions as a UV-activated colorimetric oxygen sensor. Compared to the other types of oxygen indicators, this visual oxygen indicator featuring resistance to dye leak, in-pack activation, irreversibility, reusability, and a long-shelf life will attract more interest from food and pharmaceutical industry.

Acknowledgements

This study was supported by grants from the National Research Foundation (NRF) via the National Leading Research Laboratory (NRF-2013R1A2A1A05005468); the Intelligent Synthetic Biology Center of Global Frontier R&D Project (2011-0031957); the Agriculture Research Center Program of the Ministry of Agriculture, Food and Rural Affairs (ARC-710003-03); the New & Renewable Energy of the Korea Institute of Energy Technology Evaluation and Planning (KETEP) grant funded by the Korea Government Ministry of Trade, Industry and Energy (20133030000300).

Appendix A. Supplementary data

Supplementary data associated with this article can be found, in the online version, at http://dx.doi.org/10.1016/j.snb.2015.02.084.

References

[1] C.E. Reimers, K.M. Fischer, R. Merewether, K.L. Smith Jr., R.A. Jahnke, Oxygen microprofiles measured *in situ* in deep ocean sediments, Nature 320 (1986) 741–744.
[2] A. Sin, K.C. Chin, M.F. Jamil, Y. Kostov, G. Rao, M.L. Shuler, The design and fabrication of three-chamber microscale cell culture analog devices with integrated dissolved oxygen sensors, Biotechnol. Prog. 20 (2004) 338–345.
[3] A. Mills, Oxygen indicators and intelligent inks for packaging food, Chem. Soc. Rev. 34 (2005) 1003–1011.
[4] S.-K. Lee, A. Mills, A. Lepre, An intelligence ink for oxygen, Chem. Commun. (2004) 1912–1913.

[5] S.D.F. Mihindukulasuriya, L.-T. Lim, Oxygen detection using UV-activated electrospun poly(ethylene oxide) fibers encapsulated with TiO_2 nanoparticles, J. Mater. Sci. 48 (2013) 5489–5498.
[6] S.-K. Lee, M. Sheridan, A. Mills, Novel UV-activated colorimetric oxygen indicator, Chem. Mater. 17 (2005) 2744–2751.
[7] D. Ghosh, K.G. Bhattacharyya, Adsorption of methylene blue, Appl. Clay Sci. 20 (2002) 295–300.
[8] D. Restuccia, U.G. Spizzirri, O.I. Parisi, G. Cirillo, M. Curcio, F. Iemma, F. Puoci, G. Vinci, N. Picci, New EU regulation aspects and global market of active and intelligent packaging for food industry applications, Food Control 21 (2010) 1425–1435.
[9] A. Mills, D. Hazafy, K. Lawrie, Novel photocatalyst-based colourimetric indicator for oxygen, Catal. Today 161 (2011) 59–63.
[10] A. Mills, K. Lawrie, Novel photocatalyst-based colorimetric indicator for oxygen: use of platinum catalyst for controlling response times, Sens. Actuators B 157 (2011) 600–605.
[11] C.H.T. Vu, K. Won, Bioinspired molecular adhesive for water-resistant oxygen indicator films, Biotechnol. Prog. 29 (2013) 513–519.
[12] C.H.T. Vu, K. Won, Novel water-resistant UV-activated oxygen indicator for intelligent food packaging, Food Chem. 140 (2013) 52–56.
[13] C.H.T. Vu, K. Won, Leaching-resistant carrageenan-based colorimetric oxygen indicator films for intelligent food packaging, J. Agric. Food Chem. 62 (2014) 7263–7267.
[14] A.K. Geim, K.S. Novoselov, The rise of graphene, Nat. Mater. 6 (2007) 183–191.
[15] K.P. Loh, Q. Bao, G. Eda, M. Chhowalla, Graphene oxide as a chemically tunable platform for optical applications, Nat. Chem. 2 (2010) 1015–1024.
[16] H. Zhang, X. Lv, Y. Li, Y. Wang, J. Li, P25-graphene composite as a high performance photocatalyst, ACS Nano 4 (2010) 380–386.
[17] L. Wang, K.Y. Pu, J. Li, X. Qi, H. Li, H. Zhang, C. Fan, B. Liu, A graphene-conjugated oligomer hybrid probe for light-up sensing of lectin and *Escherichia coli*, Adv. Mater. 23 (2011) 4386–4391.
[18] T. Nguyen-Phan, V.H. Pham, E.W. Shin, H.D. Pham, S. Kim, J.S. Chung, E.J. Kim, S.H. Hur, The role of graphene oxide content on the adsorption-enhanced photocatalysis of titanium dioxide/graphene oxide composites, Chem. Eng. J. 170 (2011) 226–232.
[19] J.N. Tiwari, K. Mahesh, N.H. Le, K.C. Kemp, R. Timilsina, R.N. Tiwari, K.S. Kim, Reduced graphene oxide-based hydrogels for the efficient capture of dye pollutants from aqueous solutions, Carbon 56 (2013) 173–182.
[20] S.T. Yang, S. Chen, Y. Chang, A. Cao, Y. Liu, H. Wang, Removal of methylene blue from aqueous solution by graphene oxide, J. Colloid Interface Sci. 359 (2011) 24–29.
[21] Y. Li, Q. Du, T. Liu, X. Peng, J. Wang, J. Sun, Y. Wang, S. Wu, Z. Wang, Y. Xia, L. Xia, Comparative study of methylene blue dye adsorption onto activated carbon, graphene oxide, and carbon nanotubes, Chem. Eng. Res. Des. 91 (2013) 361–368.
[22] Y.X. Xu, H. Bai, G.W. Lu, C. Li, G.Q. Shi, Flexible graphene films via the filtration of water-soluble noncovalent functionalized graphene sheets, J. Am. Chem. Soc. 130 (2008) 5856–5857.
[23] J.S. Lee, K.H. You, C.B. Park, Highly photoactive, low bandgap TiO_2 nanoparticles wrapped by graphene, Adv. Mater. 24 (2012) 1084–1088.
[24] A. Mills, D. Hazafy, Nanocrystalline SnO_2-based, UVB-activated, colourimetric oxygen indicator, Sens. Actuators B 136 (2009) 344–349.
[25] L.B. Rockland, Saturated salt solutions for static control of relative humidity between 5 °C and 40 °C, Anal. Chem. 32 (1960) 1375–1376.
[26] A. Mills, D. Hazafy, A solvent-based intelligent ink for oxygen, Analyst 133 (2008) 213–218.
[27] A. Mills, K. Lawrie, J. Bardin, A. Apedaile, G.A. Skinner, C. O'Rourke, An O_2 smart plastic film for packaging, Analyst 137 (2012) 106–112.
[28] D. Zhang, L. Fu, L. Liao, B. Dai, R. Zou, C. Zhang, Electrochemically functional graphene nanostructure and layer-by-layer nanocomposite incorporating adsorption of electroactive methylene blue, Electrochim. Acta 75 (2012) 71–79.
[29] Y. Yan, M. Zhang, K. Gong, L. Su, Z. Guo, L. Mao, Adsorption of methylene blue dye onto carbon nanotubes: a route to an electrochemically functional nanostructure and its layer-by-layer assembled nanocomposite, Chem. Mater. 17 (2005) 3457–3463.
[30] J.H. Kim, H.J. Lee, H. Jung, H.-K. Song, H.H. Yoon, K. Won, Direct electron transfer of glucose oxidase and carbon nanotubes entrapped with biocompatible organic materials, Mol. Cryst. Liq. Cryst. 519 (2010) 82–89.
[31] W.A. Hayes, C. Shannon, Electrochemistry of surface-confined mixed monolayers of 4-aminothiophenol and thiophenol on Au, Langmuir 12 (1996) 3688–3694.
[32] K. Lawrie, A. Mills, D. Hazafy, Simple inkjet-printed, UV-activated oxygen indicator, Sens. Actuators B 176 (2013) 1154–1159.

Biographies

Eun Jin Son is currently studying at the Department of Materials and Science Engineering at Korea Advanced Institute of Science and Technology (KAIST) as a Ph.D. candidate after receiving her B.S. in Materials and Science Engineering from Hanyang University, Seoul, Korea in 2012.

Joon Seok Lee received his Ph.D. in Materials and Science Engineering from KAIST in 2012. He is currently a post-doctoral researcher at Argonne National Laboratory as a Director's Post-doctoral Fellowship Recipient.

Minah Lee earned her Ph.D. on 'Design of materials for bio-inspired energy conversion and storage' in Materials and Science Engineering from KAIST in 2015

Chau Hai Thai Vu obtained her B.S. from Ho Chi Minh City University of Technology directly under Vietnam National University (Vietnam). She gained her master's degree on 'Development of water-resistant UV-activated oxygen indicator using biopolymers' from Dongguk University (Seoul, Korea) in 2012.

Hana Lee graduated from Dongguk University (Seoul, Korea) with a bachelor's degree in Chemical and Biochemical Engineering in 2013. She is now pursuing a M.S. on oxygen indicators and sensors at the same university.

Keehoon Won earned his Ph.D. in Chemical Engineering from Pohang University of Science and Technology (POSTECH), Korea in 2001. After conducting his postdoctoral research at the University of California, Berkeley (USA), he worked as senior researcher at Korea Research Institute of Chemical Technology (Daejeon, Korea). He is currently an associate professor at the Department of Chemical and Biochemical Engineering, Dongguk University (Seoul, Korea).

Chan Beum Park joined Department of Materials Science and Engineering at KAIST as an assistant professor in 2006 and is currently a KAIST chair professor since 2013. He received his B.S., and M.S., and Ph.D. from POSTECH in 1991, 1995, and 1999, respectively. Afterwards, he was a post-doctoral researcher at UC Berkeley and was an assistant professor at Arizona State University from 2002 to 2006. He was awarded Collaborative Research Award in 2015, People Glorifying Korea (hanbitsa) in 2014, Prime Minister's Award in 2013, and Technology Innovation Award (Grand Prix), etc.